Regeneration of diaphragm with bio-3D cellular patch

張, 秀英

https://doi.org/10.15017/4060034

出版情報：九州大学, 2019, 博士（医学）, 課程博士
バージョン：

Biomaterials 167 (2018) 1–14

Contents lists available at ScienceDirect

Biomaterials

journal homepage: www.elsevier.com/locate/biomaterials

Regeneration of diaphragm with bio-3D cellular patch

Xiu-Ying Zhang [a, *], Yusuke Yanagi [a], Zijing Sheng [b], Kouji Nagata [a], Koichi Nakayama [c, **], Tomoaki Taguchi [a]

[a] Department of Pediatric Surgery, Reproductive and Developmental Medicine, Graduate School of Medical Sciences, Kyushu University, 3-1-1 Maidashi, Higashi-Ku, Fukuoka, 812-8582, Japan
[b] Division of Neurofunctional Genomics, Department of Immunobiology and Neuroscience, Medical Institute of Bioregulation, Kyushu University, 3-1-1 Maidashi, Higashi-ku, Fukuoka, 812-8582, Japan
[c] Department of Regenerative Medicine and Biomedical Engineering, Faculty of Medicine, Saga University, Honjyo 1-chome, Honjyo-cho, Saga, 840-8502, Japan

ARTICLE INFO

Article history:
Received 8 January 2018
Received in revised form
7 March 2018
Accepted 8 March 2018
Available online 9 March 2018

Keywords:
Tissue engineering
Bio-3D printer
Scaffold-free cellular patch
Congenital diaphragmatic hernia
Transplantation
Skeletal muscle regeneration

ABSTRACT

Neonates with congenital diaphragmatic hernia often require surgical defect closure with a patch. Alternatives to native diaphragmatic tissue are critically needed for this paediatric surgery. The clinical efficacy of mesh patches is limited by complications associated with residual foreign material and by hernia recurrence. In this study, we used a novel bio-3D printer method to generate large scaffold-free tissue patches composed of human cells. The resulting large tissue constructs had high elasticity and strength. Cellular patches were transplanted into rats with surgically created diaphragmatic defects. Rats survived for over 710 days after implantation of tissue constructs. CT confirmed complete tissue integration of the grafts during rat growth. Histology revealed regeneration of muscle structure, neovascularization, and neuronal networks within the reconstructed diaphragms. Our results demonstrate that created cellular patches are a highly safe and effective therapeutic strategy for repairing diaphragmatic defects, and thus pave the way for a clinical trial.

1. Introduction

The diaphragm is an essential mammalian skeletal muscle and is important in respiration. In neonates with congenital diaphragmatic hernia (CDH), the diaphragm does not form properly. CDH occurs in 3.30 per 10,000 total births [1,2]. Unfortunately, there are no viable alternative therapies for these patients [3,4]; large defects often require surgical closure with synthetic patches [3] [5]. However, patch repair of CDH is associated with a high rate of hernia recurrence and can result in thoracic deformity, because the synthetic material does not grow with the infant [6,7]. In addition, the use of prosthetic materials, which are foreign substances, may lead to granulation, allergic reaction, infection, and small bowel obstruction [8,9]. Therefore, the ideal mesh remains elusive. Our research group reported effective diaphragmatic repair with an abdominal muscle flap; however, abdominal wall weakness was an associated complication [10]. There is a great need in paediatric surgery for large patches that can grow with the individual [11], and for patches made without foreign material.

Recently, tissue-engineering therapies have been introduced that use regenerated tissue as an alternative treatment for damaged tissue. Bio-3D printing has been developed to create these tissues [12,13]. Our research group developed a novel method to create scaffold-free tubular tissue from multicellular spheroids (MCS) using a bio-3D printer-based system [14,15]. Cells on 3D culture form MCS, which can better reflect in vivo physiological conditions than cells cultured in two dimensions. This method, which uses a temporary immobilization support structure to produce tissues that consist only of cells without foreign material, positions various cells in an arbitrary 3D space.

The purposes of this study were to generate scaffold-free tissues composed of human cells with our bio-3D printer method, to examine the tensile strength of these tissues, and to implant the generated tissues into diaphragmatic defects in a rat model of CDH, with a focus on survival, physiology, and safety after

* Corresponding author.
** Corresponding author. Department of Regenerative Medicine and Biomedical Engineering, Faculty of Medicine, Saga University, Honjyo 1-chome, Honjyo-cho, Saga, 840-8502, Japan.
E-mail addresses: xiuying@pedsurg.med.kyushu-u.ac.jp (X.-Y. Zhang), nakayama@me.saga-u.ac.jp (K. Nakayama).

https://doi.org/10.1016/j.biomaterials.2018.03.012

transplantation. We demonstrated that the created tissue allowed long-term survival in the rat model. The tissue was especially safe and physiologically effective during growth and development.

2. Materials and methods

2.1. Cell lines and media

Normal human dermal fibroblasts (NHDF, CC-2509), human umbilical vein endothelial cells (HUVEC, C2517A), and media were purchased from Lonza. HUVEC were grown and maintained in endothelial cell basal medium (EBM); NHDF were maintained and cultured in fibroblast basal medium (FBM). Both cultures were grown with growth supplement (Lonza). HUVEC were grown and coated with StemSure® 0.1 w/v% gelatine solution (Wako). Cells were incubated at 37 °C in 5% CO_2 and were used at passage 5–10. All cell lines are guaranteed to test negative for mycoplasma, bacteria, yeast, and fungi. All cell lines are characterized by morphological observation throughout serial passages. A certificate of analysis is provided by Lonza for each cell lot.

2.2. Preparation of multicellular spheroids

Following incubation at 37 °C under 5% CO_2 for 5 days, the cells adhering to the bottom of the dish were washed with PBS (Gibco), harvested with TrypLE™ Select (Gibco), and centrifuged. After the supernatant was decanted, mixed-cell suspensions (total cell counts of 2×10^4, 2.5×10^4, and 3×10^4) composed of HUVEC (10–30%) and NHDF (70–90%) were plated into each well of ultra-low attachment round-shaped 96-U-well plates (Sumitomo Bakelite, Tokyo, Japan), filled with mixed media of EBM and FBM at a 1:1 ratio. After 24 or 48 h, the cells aggregated to form round MCS. According to the automated measurement function of our robotic automatic cell culture system (Shibuya Kogyo Co. Ltd. Japan) and bio-3D printer, the size of the MCS (3×10^4 cells) was 662.1 ± 51.5 μm (mean ± SD) in 960 wells.

2.3. Bio-3D printer for creating tissue constructs from MCS

We used a Regenova® bio-3D printer with the Kenzan method (Cyfuse Biomedical K·K. Japan) [16,17] to assemble MCS to construct scaffold-free fibroblast sheets, short tubular tissue, and long tubular tissue. According to a 3D structure predesigned by computer, the bio-3D printer skewers MCS into a 26×26-needle array to create a fibroblast sheet. A 9×9-needle array and a 34×34-needle array were used to create short and long tubular tissues, respectively. The MCS were aspirated from the 96-well plate with a robotically controlled fine suction nozzle and inserted into the needle array made of multiple medical-grade stainless needles. All MCS were robotically positioned in a 3D structure according to the pre-designed configuration. The time required for the placement was approximately 3 h for fibroblast sheets, 1.5 h for short tubular tissue, and 3 h for long tubular tissue. The needle array was removed 7 days after placement for fibroblast sheets, 4 days after placement for short tubular tissue, and 7 days after placement for long tubular tissue.

Next, the fibroblast sheet was cultured in a sandwich-like fixing system that we developed independently. The medium was changed every 3 days for 3 weeks until the sheet was analysed. The short tubular tissue was mounted on a bioreactor (MASterflex L/S model 7519–06). The bioreactor has a 14-gauge plastic catheter (Terumo, Tokyo, Japan) with side holes. The outer diameter of each catheter was 2.1 mm. The catheter was placed inside the tubular tissue, and the system was perfused with the mixed media of FBM and EBM at a ratio of 1:1. Experiments were conducted under the same flow velocity conditions without adjustment.

In a preliminary study, when we used the same flow velocity during long tubular tissue creation, we found that the tensile strength in the resulting tissue was weak (Data not shown). Thus, we developed a method we call Tidal Currents Culture. Tidal Currents Culture carefully adjusts the flow velocity of the bioreactor. The rate was 4 ml/min for the first week and 6–8 ml/min for the following 2 weeks. From the fourth week until the fifth week the flow velocity was adjusted to 10–15 ml/min. At the sixth week, the velocity was lowered to 6–8 ml/min. From the seventh week until implantation, tubular tissue was cultured at a low flow velocity of 4 ml/min. The flow rate was empirically chosen to avoid destruction of tubular tissue resulting from high shear stress.

2.4. Tensile strength test

The tensile strength of the fibroblast sheets, short tubular tissue, and long tubular tissue were tested with a cyclic tension test, applied with a tensometer (Tissue Puller-560 TP; Bio Research Center), according to manufacturer's instructions. The maximum tensile strength of mouse diaphragm, rat diaphragm, and tubular tissue were measured in planar conditions. In brief, to display the results as a stress–strain graph, we first measured the sample length, thickness, and diameter and then stretched the sample with a target velocity of 50 μm/s. The samples were subjected to cyclic tension loading until failure. The force on the sample was plotted with MyoPULL software, which created a force–displacement curve.

2.5. Assessment of spheroid morphology with CellPRO image processor

MCS were cultured for 48 h and then spheroid diameter, circularity, and smoothness were evaluated with CellPRO image processor (Shibuya Kogyo Co. Ltd. Japan). We classified circularity into four categories: circularity ≥ 0.6 and < 0.7, ≥ 0.7 and < 0.8, ≥ 0.8 and < 0.9, and ≥ 0.9 and < 1.0. A circularity value of 1 (maximum) indicated that the spheroid was perfectly circular. Lower values indicated less circularity.

2.6. Flow cytometry analysis

The viability of MCS that contained 3×10^4 cells (10% HUVEC and 90% NHDF) was analysed. To create this condition, MCS were cultured for 48 h in mixed media of EBM and FBM and then 1×10^6 cells were collected and centrifuged. The cells were added to a water bath with TrypLE™ Select at 37 °C until the cell mass fell apart. The processing time was set to a maximum of 15 min; further processing was not performed. Next, 10% FBS (SAFC) was added to the cell solution, the solution was centrifuged at 1000 rpm for 5 min, and the resulting supernatant was removed. Then 1.5 ml PBS was added to the cells, and was filtered into FACS™ tubes. We added 500 μl of the cell solution to 'control' or '7-AAD' tubes, and then 5 μl of 7-AAD staining solution (BD Pharmingen, 559925) was added to the labelled sample. The tubes were incubated for 30 min at 4 °C in the dark prior to analysis. We set the stop count on the viable cells from a dot plot of forward scatter versus 7-AAD. Measurement and analysis of the sample were performed with FACSVerse (BD Bioscience). 7-AAD can be excited at 488 nm with an argon laser. It has a relatively large Stokes shift, emitting at a maximum wavelength of 647 nm.

2.7. Cell viability assay

Because of technical limitations, creating tubular tissue from

MCS required 3 h under room-temperature conditions. To determine the effects of exposure to room temperature, cell viability was assessed with cellular ATP measurement (CellTiter-Glo 3D cell viability assay; Promega Corporation). After 48 h of culture, MCS were moved to room temperature for 3 h. Control cells remained incubated in medium. Cells were then returned to the original cell plate, 100 μl of CellTiter-Glo reagent was added, and the plate was shaken at room temperature for 5 min before incubation at room temperature for an additional 30 min, after which the luminescent signal was quantified.

2.8. Lactate dehydrogenase assay

Lamination of the spheroids by inserting them into needle arrays to create clusters of fused fibroblasts could damage the cells within the spheroids. During the lamination process, tissue storage was in a PBS-based fixative. After lamination for 3 h, the total volume of PBS was collected and centrifuged at 1000 rpm for 5 min. Supernatants were collected and transferred to new tubes. Control spheroids were created under the same culture conditions as for long tubular tissue, but without the use of the needle array. An ELISA LDH cytotoxicity detection kit (Takara Bio Inc.) was used to determine the percentage of LDH released in the protocol. To determine the maximal LDH release, cells were treated with 1% Triton X-100.

2.9. Histology and immunohistochemistry

We performed morphological analysis on samples, including MCS after 48-h culture, cell sheets after 3 weeks' culture, tubular tissue after 7 weeks' culture, normal rat diaphragm, regenerated rat diaphragm, and secreted collagen (in culture medium). Samples were fixed with 4% formalin for 48 h, then embedded in paraffin and cut into 2-μm (MCS) and 3-μm slices. The nuclei were counterstained with HE. To visualize collagenous connective tissue fibres, the paraffin-embedded sections were stained with Masson's trichrome. To detect elastic fibres, elastica van Gieson (EVG) staining was performed. To detect microvessels, we performed immunohistochemistry analysis for vascular endothelial cell marker CD31, using anti-CD31 antibody (1:50, ab28364, Abcam). To detect diaphragm muscle using the marker desmin, *anti*-desmin antibody (1:100; D33, ab8470, Abcam) was used. To detect collagen I, COL1A1 (D-13) was used (1:200; Santa Cruz Biotechnology). The neuron marker HuC/HuD antibody was used (1:300; A-21271, Thermo Fisher Scientific). For a synaptic vesicle marker, *anti*-synaptophysin antibody was used (1:500; ab14692, Abcam). To detect the axons of neurons, anti-MAP2 antibody was used (1:500; M4403, Sigma-Aldrich). In brief, sections were deparaffinized, incubated for 30 min with 0.3% hydrogen peroxide/methanol to block endogenous peroxidase activity, and then incubated with primary antibodies at 4 °C overnight. An ImmPRESS reagent kit was used. All sections were visualized with 3,3′-diaminobenzidine (DAB).

2.10. Fluorescence immunohistochemistry

To inactivate endogenous peroxidase, samples were incubated in hydrogen peroxide with methanol, and then blocked with 10% goat normal serum (Histofine SAB-PO kit) for 1 h at room temperature. Anti-vimentin antibody (1:100; ab16700, Abcam) recognizes only human vimentin [18]. Anti-desmin antibody (1:100; D33, ab8470, Abcam), *anti*-VEGF receptor antibody (1:300; ab32152, Abcam), rabbit anti-ChAT antibody (1:500; Chemicon), and anti-tyrosine hydroxylase antibody (1:750; ab112, Abcam) were used. Antibodies reacted overnight at 4 °C. The corresponding secondary antibodies—goat anti-mouse IgG H&L (Alexa Fluor® 594, ab150116, Abcam) and goat anti-rabbit IgG H&L (Dylight® 488, ab96899, Abcam)—were then added and incubated for 1 h at room temperature. Nuclei were counterstained and DAPI images were obtained with an inverted LSM700 META confocal microscope (Carl Zeiss).

2.11. Diaphragmatic defect rat model and surgical transplantation procedures

Animals: Male F344/N-rnu nude rats (8–12 weeks of age; CLEA, Japan) were divided into a normal group and three CDH groups. The three CDH groups were: 1, no repair group, in which diaphragmatic defects were not repaired (n = 3); 2, Vicryl mesh repair group (n = 6), in which diaphragmatic defects were repaired with Vicryl mesh (Ethicon); and 3, cellular patch repair group (n = 5), in which diaphragmatic defects were repaired with created tissue. All animals were maintained in an air-conditioned, specific-pathogen-free room with time-controlled lighting. Animal handling and euthanasia were in accordance with national prescribed guidelines. The number of the animals was based on the guiding principles underpinning the humane use of animals in scientific research (replacement, reduction, refinement). Ethical approval for the study was granted by the Animal Experiment Committee of Kyushu University (approval number: A25-053-1; A27-093-2). Rats were randomized allocated to the experimental groups. No inclusion/exclusion criteria were used, no samples or animals were excluded from the analysis. Observers blind to the experiment.

Surgical procedures: Diaphragmatic defects were surgically created. All surgeries were performed under sterile conditions, with continuous monitoring of heart rate and oxygen saturation (PhysioSuite; Kent Scientific). Implant surgeries were performed under general anaesthesia. Anaesthesia was induced with isoflurane inhalation, followed by an intraperitoneal injection of butorphanol (Meiji Seika, Japan), medetomidine (Nippon Zenyaku Kogyo Co. Ltd.), and midazolam (Teva Pharma, Japan), mixed in a single syringe, to enhance sedation and analgesia. The rats were intubated with 16-gauge indwelling catheters and mechanically ventilated. Laparotomy was performed through a subcostal incision. A 12 × 10-mm rectangular defect was created in the left diaphragm [19,20]. (A clinical study reported that approximately 80% of CDH are left-sided defects [5]. The defect was repaired with Vicryl mesh or cellular patch (tubular tissue) and sutured with a 6–0 nonabsorbable suture (PROLENE; Johnson & Johnson Medical Limited). Animals were allowed food and water after the procedure. All surgical interventions were performed in a semi-sterile environment using tip-sterilized surgical instruments, and sterile equipment.

2.12. Oxygen saturation

We assessed SpO_2 in room air with a PhysioSuite monitor for rats (Kent Scientific). Rats were monitored under general anaesthesia with isoflurane. Measurements were taken just before awakening to avoid the effects of anaesthesia. Each measurement was finished quickly; the value of SpO_2 was used for analysis.

2.13. Computed tomography (CT) images

To evaluate and characterize the regenerated diaphragm in living animals, the rats underwent micro-CT imaging (Rigaku, Tokyo, Japan). All rats were anaesthetized with isoflurane prior to and throughout the scans. The x-ray tube voltage, current, and field of view were according to the described protocol. In animal studies in terms of histology, SpO2, and CT images analysis were performed in a single-blind fashion.

2.14. Statistical analysis

Statistical analysis was performed with JMP® Pro 13.0.0. Means, standard deviations, and the probability (P) associated with a Student's *t*-test, Tukey-HSD test using a two-tailed distribution of equal variance are shown in some figures. Statistical analysis was performed on groups with similar variance. P values < 0.05 were considered statistically significant. No samples were excluded specifically from analysis.

2.15. Data availability

All relevant data included in this study are available from the corresponding author upon reasonable request.

3. Results

3.1. Creating sheet-shaped scaffold-free fibroblast constructs

To create sheet-shaped scaffold-free fibroblast constructs with a bio-3D printer, we first created round MCS from fibroblasts, then skewered the MCS onto needle-shaped materials according to the Kenzan method (Supplementary Fig. 1A). The sheet measured approximately $4 \times 5 \times 1$ mm (Supplementary Fig. 1B). Haematoxylin and eosin (HE) staining revealed normal cell morphology (Supplementary Fig. 1C) and homogeneous distribution of cells within the sheet-shaped scaffold-free fibroblast construct (Supplementary Fig. 1D). However, the tensile strength of the sheet was not adequate for transplantation (Data not shown). These results indicate that the fibroblasts formed cell–cell adhesion with the bio-3D printer.

3.2. Construct composed only of human cells

To improve the tensile strength of the transplanted tissue, we developed a method that provided the culture with a circulation system. We used a 3D tube-shaped structure pre-designed on a computer system and plotted in green (Fig. 1A), laminated the MCS to a Kenzan needle array to create tubular tissue, then cut a patch from the tubular tissue to repair the diaphragm defect (Fig. 1A).

After Kenzan culture on a 9×9-needle array for 5 days, a total of 560 MCS made of fibroblasts cells had fused to a height of 12.5 mm (Fig. 1B). These were mounted on a bioreactor with circulation (Fig. 1C). After 3 weeks of culture, a long tube of tissue had formed, approximately 5 mm long and approximately 1 mm thick, with an inner diameter of approximately 3 mm. The tubular tissue had a smooth surface and likely had greater elasticity than the fibroblast sheets (Fig. 1D). During tissue creation, the cell-fusion-induced shrinkage rate was about 50–60%. We tested tensile strength with a cyclic tension test, and created a force–displacement curve that included an elastic region, a destructive change region, and the failure point [21]. The maximal force was approximately 64 mN after 10 days of culture and approximately 231 mN after 3 weeks of culture (Fig. 1E). From these results, we concluded that the created tubular tissue had relatively high elasticity and strength.

3.3. Tubular tissue with high elasticity and tensile strength

We needed larger, stronger tissue for transplantation, and therefore we co-cultured human umbilical vein endothelial cells (HUVEC) and normal human dermal fibroblasts (NHDF). It was recently reported [22,23] that HUVEC produced endothelial tubes with a lumen while NHDF secreted necessary matrix; the combination could therefore be a novel tube formation system.

In preliminary analysis of the quality of spheroids in the tubular tissue, MCS were markedly homogeneous, compact, and circular at confluence (Supplementary Fig. 2A and B). We analysed the spheroids by staining them with HE, CD31, Masson's trichrome, and collagen I (Supplementary Fig. 2C, D, E, F), which clearly revealed that the cell source had high quality. Because of a technical limitation, making MCS required 3 h at room temperature (Supplementary Video 1); 7-AAD assay revealed that approximately 98% of cells survived (Supplementary Fig. 2G). There was no difference in cell viability between the control group and the group exposed to room-temperature conditions ($P > 0.05$) (Supplementary Fig. 2H). Although the Kenzan needles damaged cells within the spheroids, fewer than 0.8% of cells were damaged, according to cytotoxicity activity on a lactate dehydrogenase (LDH)-release assay (Supplementary Fig. 2I). These results provide evidence that only slight cell damage occurred, and that this damage did not affect the quality of the created tissue.

Supplementary video related to this article can be found at https://doi.org/10.1016/j.biomaterials.2018.03.012.

To create long tubular tissue, we used a longer Kenzan system (Fig. 2A), designed to use a 34×34-needle array. After 7 days of Kenzan culture of a total of 960 wells of MCS, when the height of the fused clusters was approximately 20 mm ($n = 3$; mean length, 21 ± 2.65 mm; Fig. 2B, Supplementary Video 1), the tissue was removed from the needle array. After an additional 7 weeks of Tidal Currents Culture (Fig. 2C), long tubular tissue had formed, approximately 8 mm in length, with an inner diameter of approximately 3 mm and a tube wall thickness of approximately 1 mm (Fig. 2D and E). During creation of the long tissue, the cell-fusion-induced shrinkage rate was about 60%. The tubular tissue had a smooth surface and a perfectly elastic structure. To evaluate tensile strength, we prepared two types of long tubes. One type was composed of 70% NHDF and 30% HUVEC; this type withstood a maximal force of approximately 594 mN (Fig. 2F). The second type was composed of 90% NHDF and 10% HUVEC; the maximal force for this type was approximately 1430 mN (Fig. 2F). Experiments were also conducted at a 50:50 ratio of NHDF to HUVEC; however, satisfactory data were not obtained (Data not shown). Regarding the elastic region [21], tube tissue with 90% NHDF and 10% HUVEC was three times more elastic than tissue created with 70% NHDF and 30% HUVEC (Supplementary Fig. 3A). After destruction of the created tubular tissue with a tensometer, elongated collagen fibrils were clearly visible in the destroyed tissue (Fig. 2G). These results confirmed that the long tubular tissue had relatively high elasticity and strength when created with 90% NHDF and 10% HUVEC.

3.4. Formation of complex network in tissue

To identify the mechanisms underlying this high elasticity and strength, we observed morphological changes in the tubular tissue. HE staining revealed morphologically normal cells (Fig. 3A). Apoptotic cells were not found in either the outer layer (Fig. 3B) or inner layer (Fig. 3C). Cells stained positive for CD31, suggesting the presence of micro-vessels (Fig. 3D), with less expression in the outer layer (Fig. 3E) than in the middle and inner layers (Fig. 3F). CD31 concentrates at endothelial cell borders, where it engages in cell-to-cell homophilic binding. Masson's trichrome staining was positive throughout the tube (Fig. 3G), most strongly in the outer layer (Fig. 3H), but also in the middle and inner layers (Fig. 3I).

Last, spheroids produced collagen I (Fig. 3J), both within the cells and in the extracellular matrix throughout the tube (Fig. 3K). We also found collagen I released into the cell culture medium during tissue growth. We collected the medium after 4 days' culture with circulation and measured the weight (Supplementary Fig. 3B). The collected mass stained positive for collagen I (Supplementary Fig. 3C and D).

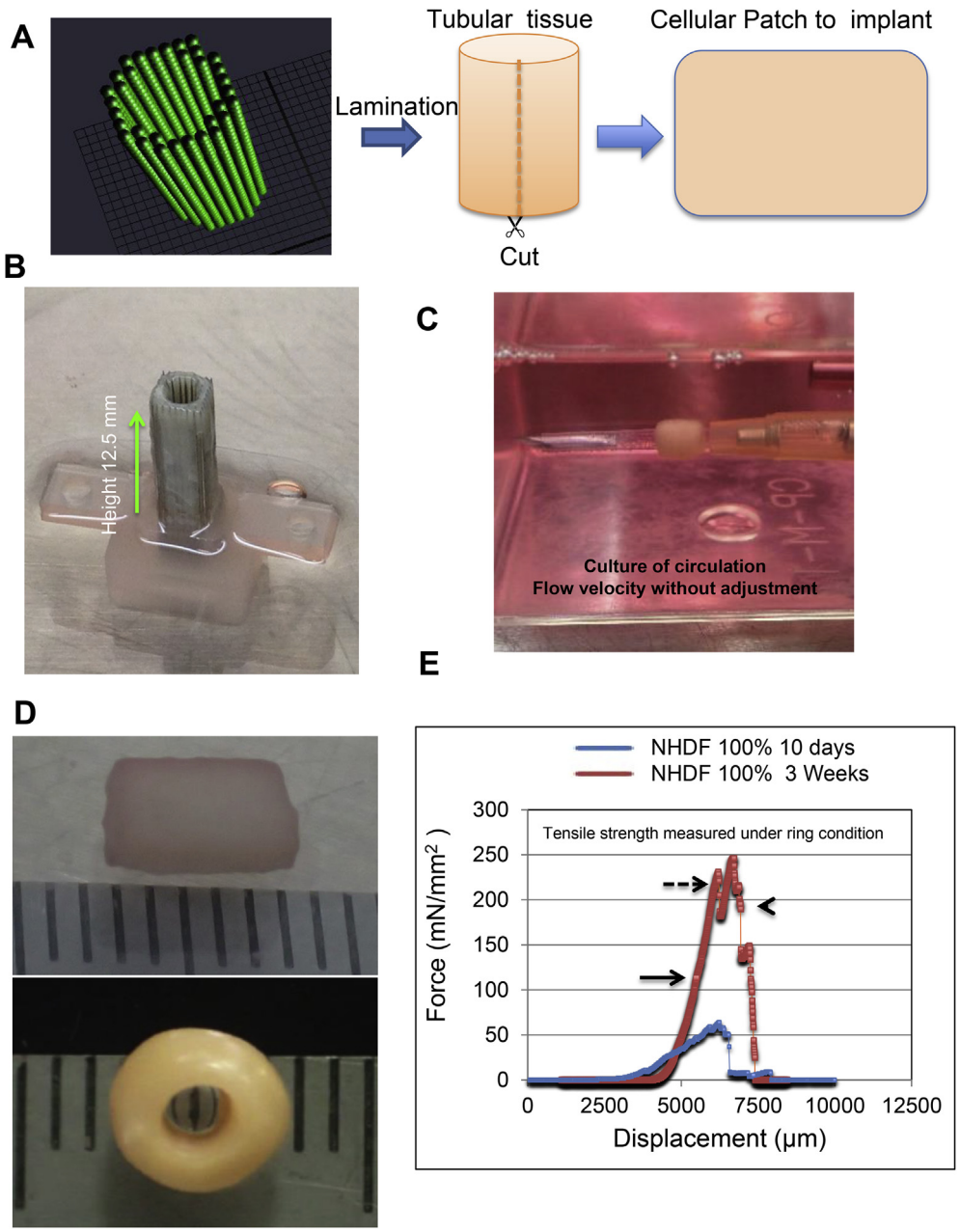

Fig. 1. Short tubular tissue created with bio-3D printer and analysis of tensile strength. (**A**) Simple schematic of method for creating a patch containing only cells. First, tubular tissue is created; the resulting tissue is cut into a patch for implantation. (**B**) Fused fibroblast clusters created with 9 × 9-needle array (total of 560 MCS) after 5 days of Kenzan culture. (**C**) Tubular tissue is mounted on a bioreactor that has a 14-gauge plastic catheter to provide circulation to the culture. Culture of circulation Flow velocity without adjustment, Flow velocity was 4 ml/min. (**D**) Example of short tubular construct (approximately 6 mm in length) created after 3 weeks of culture with circulation. (**E**) Representative force–displacement curve. Tensile strength was measured with a tensometer under ring conditions. Arrow shows the plastic region. Dashed arrow shows the region of destructive change. Arrow head shows the failure point. Data from the created tubular tissue after 10 days or 3 weeks of culture.

Collectively, these data strongly demonstrated the formation of a complex network in the tubular tissue, including micro-vessels and fibrils, with collagen in the extracellular matrix.

3.5. CDH model repair with cellular patches

To assess whether the created tubular tissue would be functionally efficient in vivo, transplantation was performed in a surgically created rat model of severe CDH. We compared normal rats, CDH rats without repair, CDH rats repaired with Vicryl mesh, and CDH rats repaired with a cellular patch. The CDH model was created through left anterolateral laparotomy (Fig. 4A–D); hernias were repaired with a Vicryl mesh (Fig. 4E) or cellular patch (Fig. 4F and Supplementary Video 2), which was sutured to the native diaphragm (Fig. 4G and H).

Supplementary video related to this article can be found at https://doi.org/10.1016/j.biomaterials.2018.03.012

We measured the tensile strength in the removed rat diaphragmatic tissue, and compared it with mouse diaphragmatic tissue (as a control) and with the created tubular tissue. The diaphragm is a sheet-shaped muscle; therefore, the created tubular tissue was cut into rectangles and tensile strength was measured in the same planar conditions (Supplementary Fig. 4). The tensile strength of the diaphragm was 96 ± 48.25 mN/mm^2 in mice and

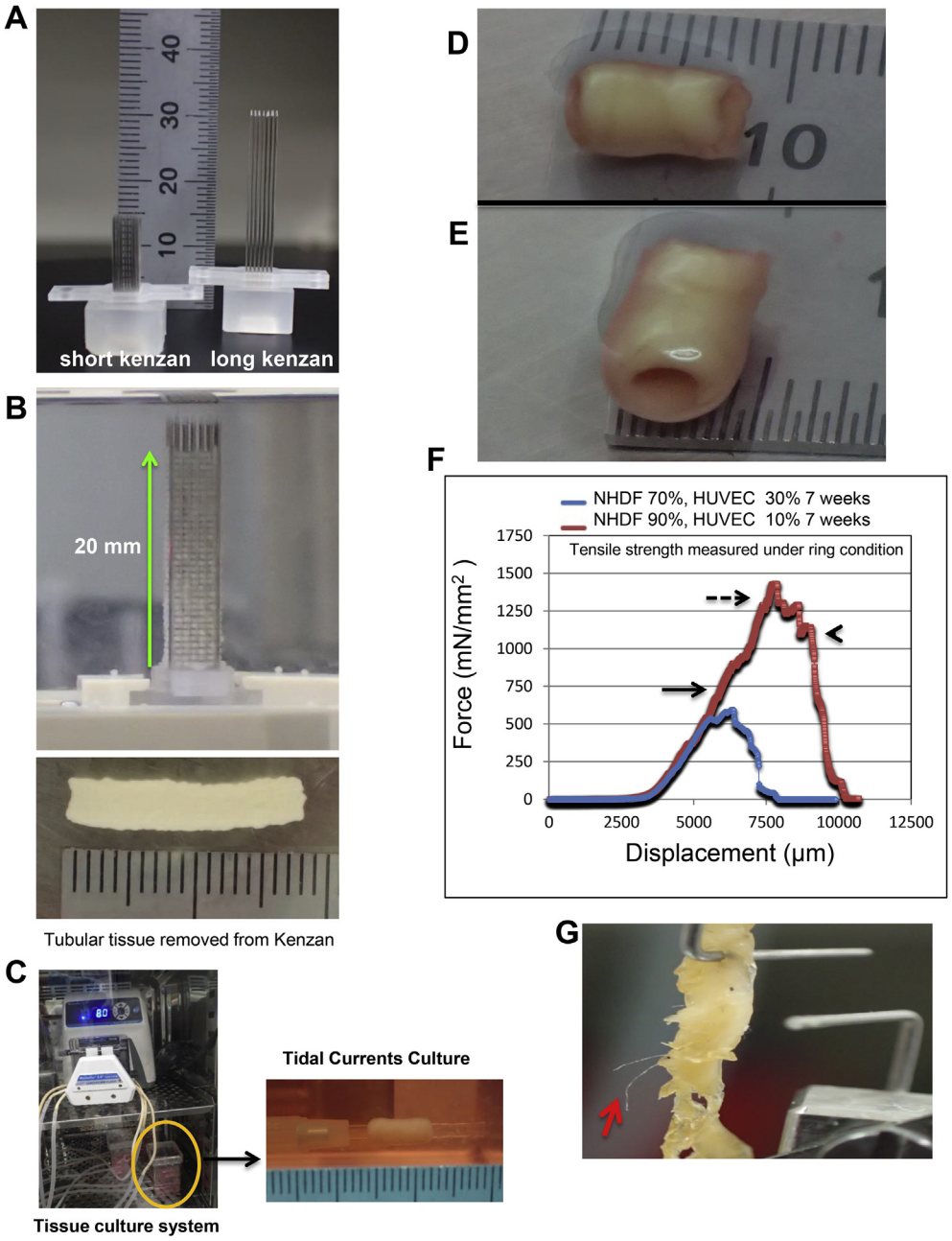

Fig. 2. Long tubular tissue created with bio-3D printer using co-culture of NHDF and HUVEC cells, and analysis of tensile strength. (A) Photographs of the short (12.5-mm) and long (26.4-mm) needle arrays used to create fused clusters. (**B**) Fused clusters (approximately 20 mm in length) of NHDF and HUVEC created with 34 × 34-needle array (total of 960 MCS) after 7 days of Kenzan culture. The effective created length in three samples was 21 ± 2.65 mm after removal from needle array. The image shows a tube approximately 18 mm in length. (C) Removed tubular tissue was cultured with circulation chamber (yellow circle). (D) Length of created long tubular construct was approximately 8 mm. (E) Inner diameter was approximately 3 mm; tube wall thickness was approximately 1 mm. (F) Representative force–displacement curve. Tensile strength was measured with the tensometer under ring conditions. Dashed arrow shows the region of destructive change. Arrow head shows the failure point. (G) Collagen fibrils are clearly visible in the destroyed tissue after stretching with the tensometer. Arrow shows collagen fibrils.

375.8 ± 48.25 mN/mm^2 in rats. The tensile strength of the cellular patch was 337.75 ± 53.95 mN/mm^2. These data clearly demonstrated that the created tubular tissue had high tensile strength, similar to that of the rat diaphragm ($p > 0.05$). The tissue could thus withstand repeated surgical suturing (Supplementary Video 2) and was sufficient to repair the defect in the rat CDH model.

By 2–3 weeks after surgery, the thoracic wall scars were unremarkable, with no sign of inflammation or infection. We observed oxygen saturation (SpO_2) after transplantation (Fig. 4I). The SpO_2 was lower in the Vicryl mesh group than in the control group ($P < 0.01$). The cellular patch group had markedly higher SpO_2 levels than the Vicryl mesh group ($P < 0.01$); these levels did not differ from those in the normal group ($p > 0.05$). These experiments directly show that a functionally normal diaphragm was regenerated after transplantation.

We also carefully observed weight gain after transplantation (Fig. 4J). Three weeks after transplantation, rats showed normal weight gain. We did not observe any differences among normal, Vicryl mesh, and cellular patch groups at that time point. However, beginning at 3 weeks, the Vicryl mesh group began to have

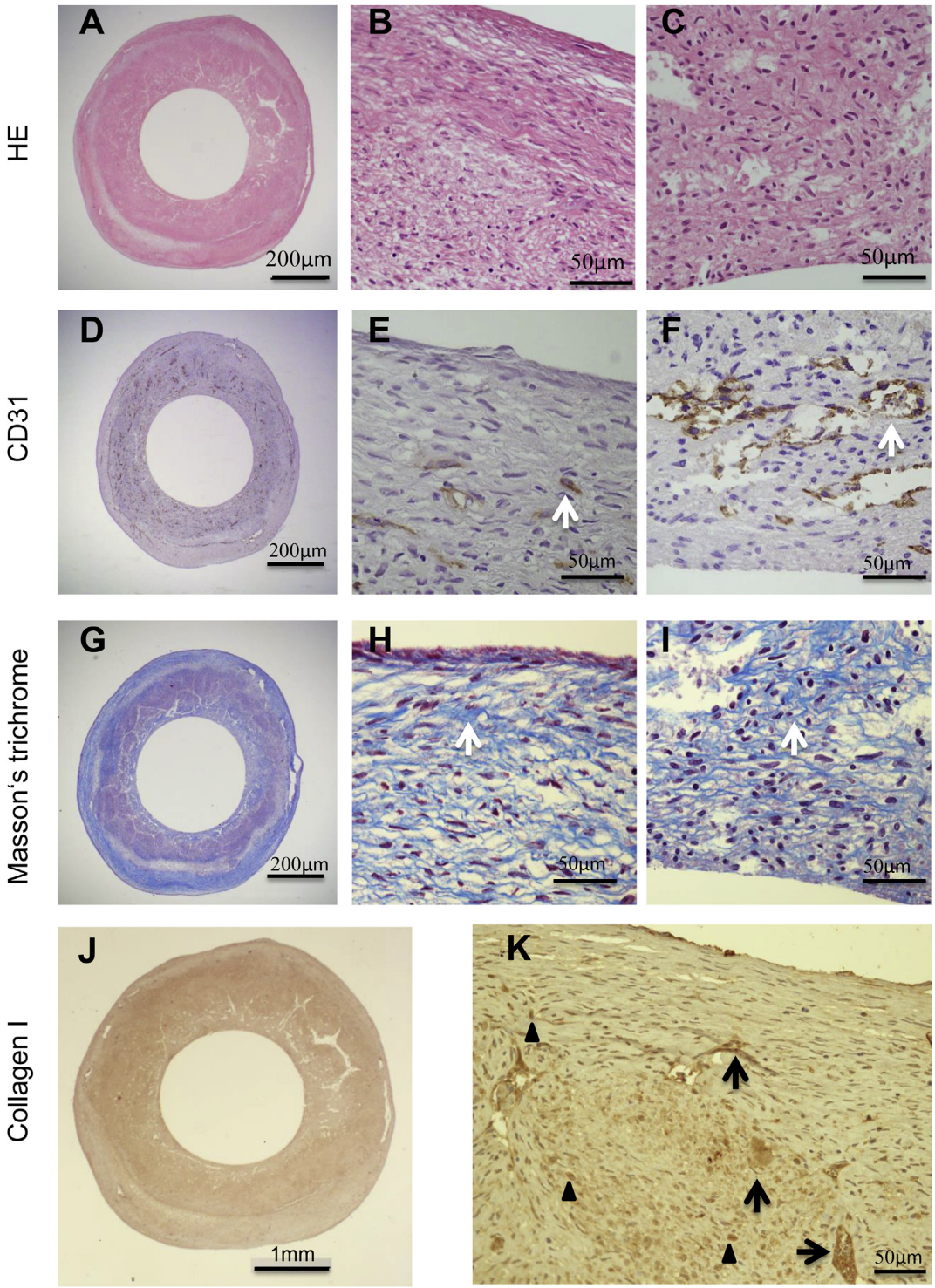

Fig. 3. Histological analysis of the tubular tissue. (A) Tubular tissue stained with haematoxylin and eosin (HE). Tissue is smooth on internal and external edges and tube is fully closed. High-power images of HE staining show morphologically normal nuclei in outer layer (B), and inner layer (C). (D) CD31 staining. Weak expression of CD31 in outer layer (E), and strong expression in middle and inner layers (F). Micro-vessels stain positive for CD31 (arrows). (G) Masson's trichrome staining. Strong expression of Masson's trichrome in outer layer (H). Weak-to-moderate expression in middle and inner layers (I). Dark, strongly stained fibrils are observed (arrows). (J) Tubular tissue stained for collagen I. (K) Collagen I is expressed within cells (arrowheads), and in the extracellular fluid throughout the tube (arrows).

persistent growth failure and death (survival fig), and we could not continue to observe body weight in that group. We continued to monitor differences in weight gain between normal and cellular patch groups to evaluate long-term effects. The cellular patch group gained body weight at a rate similar to that of the control group. Thus, after cellular patch transplantation, rats had favourable development with no effect on normal growth.

In addition, survival was recorded daily for each group after transplantation (Fig. 4K). The CDH rats without repair had a survival rate of 0% after 48 h. This survival rate was worse than that of the

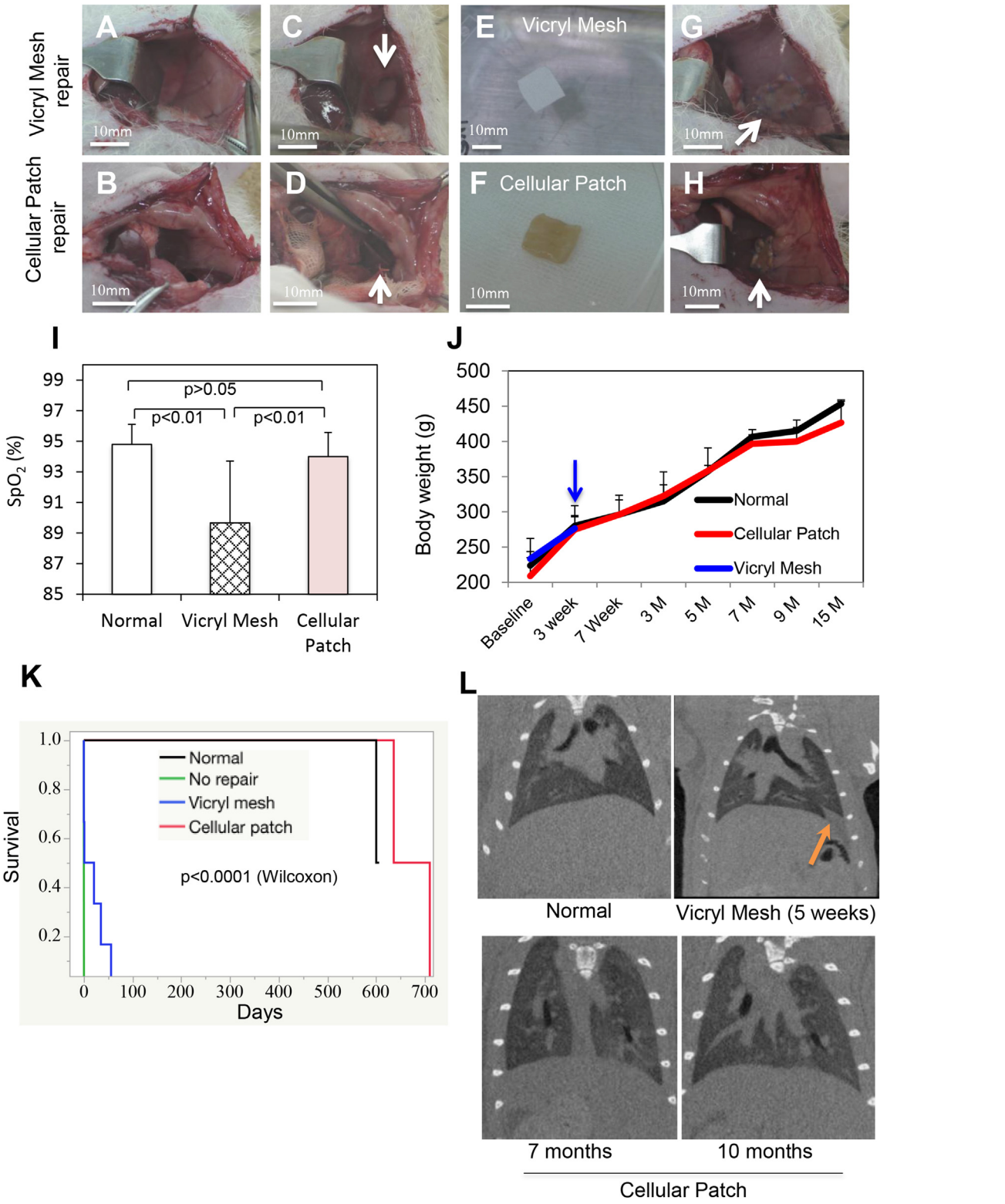

Fig. 4. Surgically created rat model of CDH and diaphragm function after cellular patch transplantation. (A), (C), (E), (G) Vicryl mesh repair group. (B), (D), (F), (H) Cellular patch transplant group. (A), (B) A surgical incision was made through the left anterolateral abdominal wall. (C), (D) A defect approximately 12 × 10 mm in size was made. Arrows show the defect in the diaphragm. (E) Vicryl mesh patch approximately 12 × 10 mm in size was implanted in diaphragm. (F) Long tubular tissue was cut into a rectangle approximately 12 × 10 mm in size and implanted in rat diaphragm. (G), (H) Suture is seen (arrows). (I) Oxygen saturation. N = 5 for normal, n = 3 for Vicryl Mesh, and n = 5 for cellular patch. P = 0.005 (normal vs. Vicryl Mesh), p = 0.007 (Vicryl Mesh vs. cellular patch), p = 0.45 (normal vs. cellular patch) by Student's t-test. (J) Changes in body weight after transplantation among normal rat, Vicryl mesh, and cellular patch transplanted groups. N = 4 for normal, n = 3 for Vicryl Mesh, and n = 4 for cellular patch. The cellular patch group gained body weight at a rate similar to that of the control group. Arrow, Vicryl mesh rat began to persistent growth failure, and observation could not be continued. (K) Kaplan-Meier survival analysis. Significantly different survival curves according to Wilcoxon test. N = 3 for normal, n = 3 for no repair, n = 6 for Vicryl Mesh, and n = 5 for cellular patch. (L) CT images show hernia occurrence in Vicryl mesh group (arrow). No hernias occurred at any time in the cellular patch group. (I), (J), (K) Error bars represent the mean ± s.d.

Vicryl mesh group. One rat in the Vicryl mesh group was still alive at 7 weeks. However, hernia had occurred in that rat (CT imaging). No mortality was recorded at any time in the cellular patch group, which maintained 100% survival. The longest survival was up to 710 days after transplantation.

Last, the function of the reconstructed diaphragm was assessed with CT imaging in the living rats (Fig. 4L). In the Vicryl mesh repair group, CT images revealed a 4 × 3-mm hernia in the left diaphragm 5 weeks after transplantation. This finding indicated that the Vicryl mesh had begun to be absorbed, and that localized weak regions had given rise to the hernia. We assessed the diaphragm with CT imaging in the cellular patch group at 1 month (n = 1), 4 months (n = 1), 7 months (n = 1), and 10 months (n = 2) after transplantation. There were no diaphragmatic hernias at 4 months (Data not shown). Over the longer term of 7–10 months, CT-scanning demonstrated that the diaphragms had a smooth surface, confirming the integrity of the cellular patch; hernias did not occur at any time.

These results suggest that the cellular patch actually integrated into the diaphragm, which prevented hernias from occurring, and that cellular patches were effective for repairing large diaphragm defects during rat development.

3.6. Presence of regenerated muscle fibres

We evaluated the survival of implanted tissue and the regeneration of muscle fibres within the reconstructed diaphragm after transplantation. After carefully opening the thoracic cavity, we found noinfection on naked-eye observation of the diaphragm. The cellular graft was successfully integrated with the diaphragm, with clearly visible areas of vascularization. Postoperative adhesions to the side of the thoracic incision had not formed and no rib cage deformation was present. Two rats had slight adhesions between the stomach and the abdominal side of the incision. We carefully distinguished graft and host regions. The implanted grafts maintained their original shapes and the non-absorbable sutures were seen (Fig. 5A). The reconstructed region was removed from the diaphragm (Fig. 5B).

HE staining in the normal group revealed diaphragm muscles with morphologically normal nuclei (Fig. 5C and D). Four months after transplantation, the reconstructed diaphragm showed clear morphologically normal nuclei and a muscle-like structure (Fig. 5E and F). Seven months after graft transplantation, the reconstructed diaphragm had more normal muscle architecture (Fig. 5G and H). No obvious pathological changes, such as cell membrane rupture or cell death, were observed in the transplanted tissue (Fig. 5F, H). Thus, our histological examination revealed regeneration, with no degeneration of the graft after transplantation.

To further evaluate the regeneration of muscle-like structure, the reconstructed diaphragm was characterized with Masson's trichrome staining analysis. The diaphragm of normal rats showed a normal distribution of collagen fibres (blue) around the muscle (red) (Fig. 5J). Four and 7 months after transplantation, rich collagen fibres and muscle cells were present in the reconstructed diaphragm, features similar to normal tissue (Fig. 5K–N). Compared to the 4-month group (Fig. 5K and L), the 7-month group showed markedly increased distribution of collagen fibres, as well as increased size of the myofibres (Fig. 5M and N).

To further test whether muscle fibres were properly formed, we evaluated the structural muscle protein, desmin. Desmin immunostaining covered the entire cytoplasmic area with clear striations in normal rat tissue, clearly confirming the presence of striated muscle (Fig. 5O). Desmin immunostaining was present at the implantation site in reconstructed diaphragms in the transplanted group (Fig. 5P and Q). After 4 months (Fig. 5P), we found that although many sheet-shaped structures were stained, indicating active regeneration of muscle cells, as seen in HE and Masson's trichrome staining (Fig. 5F, I), the size and number of muscle fibres were insufficient compared with the control striated muscle. After 7 months (Fig. 5Q), aligned, elongated, desmin-positive cells were clearly observed, indicating regeneration of the muscular layer. These desmin-positive cells tended to have a significantly wider area and increased volume compared with cells at 4 months, with muscle fibres similar to those in the normal rat. These results confirmed implanted tissue survival and regeneration of structural muscle fibres after transplantation.

3.7. Neovascularization and neuronal network

Neovascularization and neuronal network formation were evaluated in the reconstructed diaphragm after transplantation. Elastica van Gieson (EVG) staining revealed vessel wall-like structures that contained an elastic muscle layer (Fig. 6A). Four months (Fig. 6B) and 7 months (Fig. 6C) after transplantation, vessel wall-like structures were detected at the implantation site; most were markedly concentrated near muscle tissue. In the enlarged image of EVG staining, the inner elastic fibres of the blood vessel are dyed purple-black; the yellow indicates muscle (Supplementary Fig. 5A–C). Additionally, newly developed blood vessels were stained with another marker, VEGF-1 (Fig. 6D) in normal rat tissue. This staining clearly demonstrated that blood vessels were present in the reconstructed grafts (Fig. 6E and F).

We next assessed the expression of neurons to evaluate neuromuscular innervation of the reconstructed diaphragm. The acetylcholine marker ChAT identified motor nerve terminals in normal rat diaphragms (Fig. 6G). ChAT-positive cells were clearly seen in the reconstructed diaphragm at 4 (Fig. 6H) and 7 months (Fig. 6I) after transplantation. We also used MAP2 staining, which stained the cell bodies and axons of neurons in normal rat tissue (Fig. 6J). This test revealed the presence of neurons and axons in the reconstructed graft (Fig. 6K and L). Another neuronal marker (Supplementary Fig. 5D–F) and a synaptic vesicle signal marker (Supplementary Fig. 5G–I) were observed, with the same results. We also stained a sympathetic neuron marker that is reported to modulate diaphragm muscle formation and maintenance [24]. TH-positive cells were observed (Supplementary Fig. 6).

Collectively, these results indicate neovascularization and regeneration of a neuronal network within the reconstructed diaphragms after transplantation.

3.8. Human cells were integrated into the regenerated diaphragm

We further tested whether human cells were integrated into the regenerated diaphragm. First, we used a monoclonal vimentin antibody [18], which recognized human cells only (Fig. 7A) and desmin, a muscle marker, which recognized rat cells only (Fig. 7B). We double-stained the reconstructed diaphragm samples with the two antibodies 7 months after transplantation. Vimentin-positive cells derived from human cells were still clearly visible, and were localized along the regenerated striated muscle, which stained positive for desmin (Fig. 7C, upper panel). However, many desmin-positive muscle cells were negative for vimentin, and human cells were also localized in the regenerating muscle (Fig. 7C, lower panel). These findings demonstrate that human cells were integrated into the structure of the regenerated diaphragm.

4. Discussion

In the present study, we successfully used a bio-3D printer to create large constructs composed only of cells and demonstrated

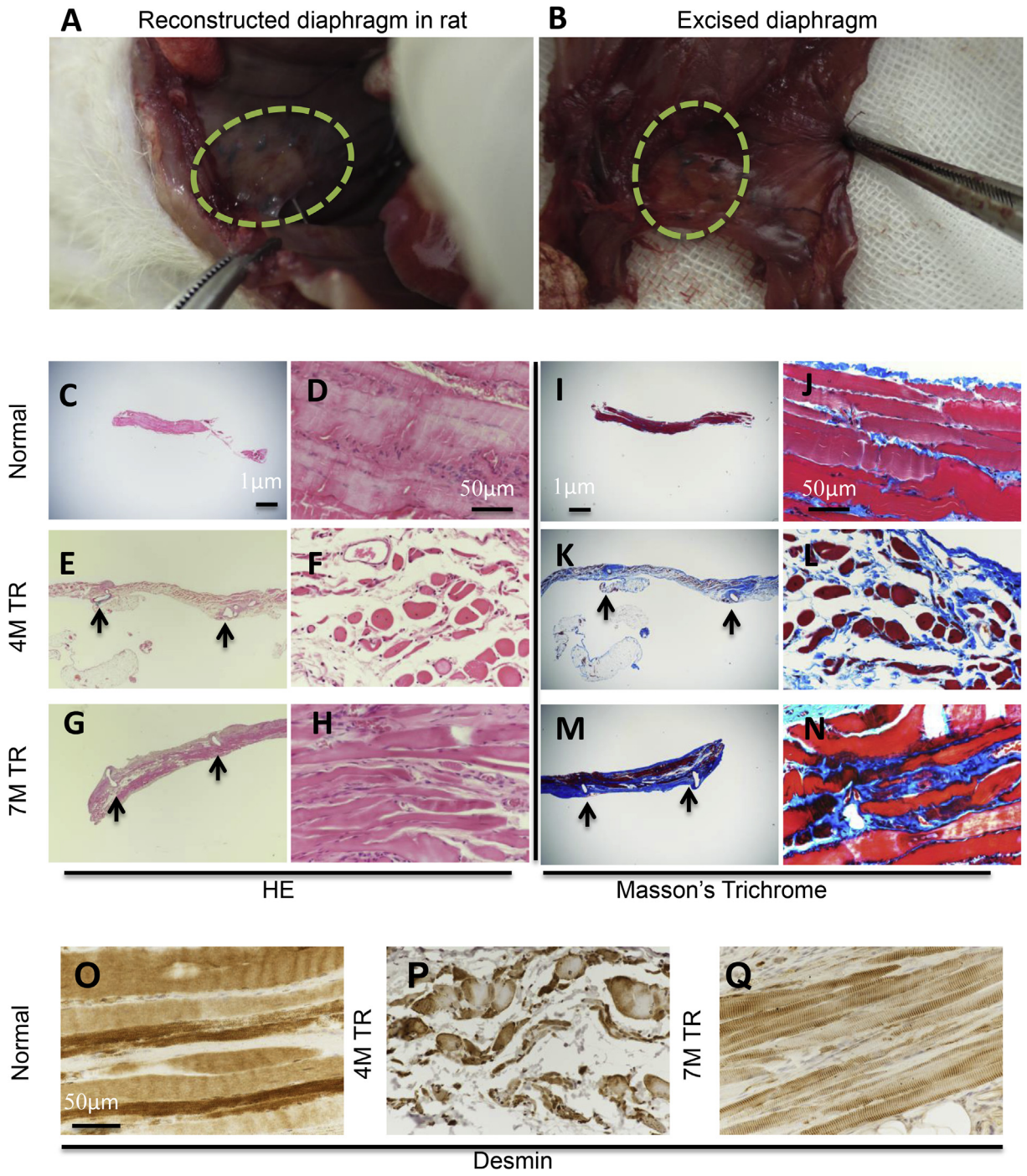

Fig. 5. Histological analysis of reconstructed diaphragm 4 and 7 months after transplantation (HE, Masson's trichrome, and desmin staining). (**A**) Photograph of implanted cellular patch in diaphragm. Dotted lines demarcate the original construct. Non-absorbable sutures are seen (black). (**B**) Reconstructed portion of diaphragm. The excised diaphragm is shown (dotted lines). (**C**)–(**H**) HE staining of normal diaphragm and of reconstructed diaphragm 4 months (4 M TR) and 7 months (7 M TR) after transplantation. Left panel, transplanted graft area is surrounded, shown by two arrows; right panel, magnified images show morphologically normal nuclei. (**I**)–(**N**) Masson's trichrome staining. Left panel, grafts in transplanted area are surrounded, shown by two arrows; right panel, magnified images show collagen fibres around the muscle observed in all three groups. Seven months after transplantation, the shape and size distribution of the myofibres is close to normal. (**O**)–(**Q**) Desmin staining. After 4 months, new muscle cells have developed in the sheet-shaped structure. After 7 months, the shape and the size distribution of the muscle tissue is close to normal.

that the resulting tubular tissue had relatively high elasticity and strength. In a surgically created experimental model of a diaphragmatic defect, the long-term survival rate was 100% 710 days after construct tissue implantation. To our knowledge, this is the first report of diaphragmatic defect repair using created grafts composed only of cells.

Absorbable grafts, such as Surgisis, and nonabsorbable grafts, such as polytetrafluoroethylene, trigger inflammation, which frequently results in patch disruption and hernia recurrence as patients grow. To overcome the shortcomings of synthetic mesh, the use of mesh as a scaffold for seeded stem cells has been reported. One group used prosthetic mesh as a scaffold in a rat model

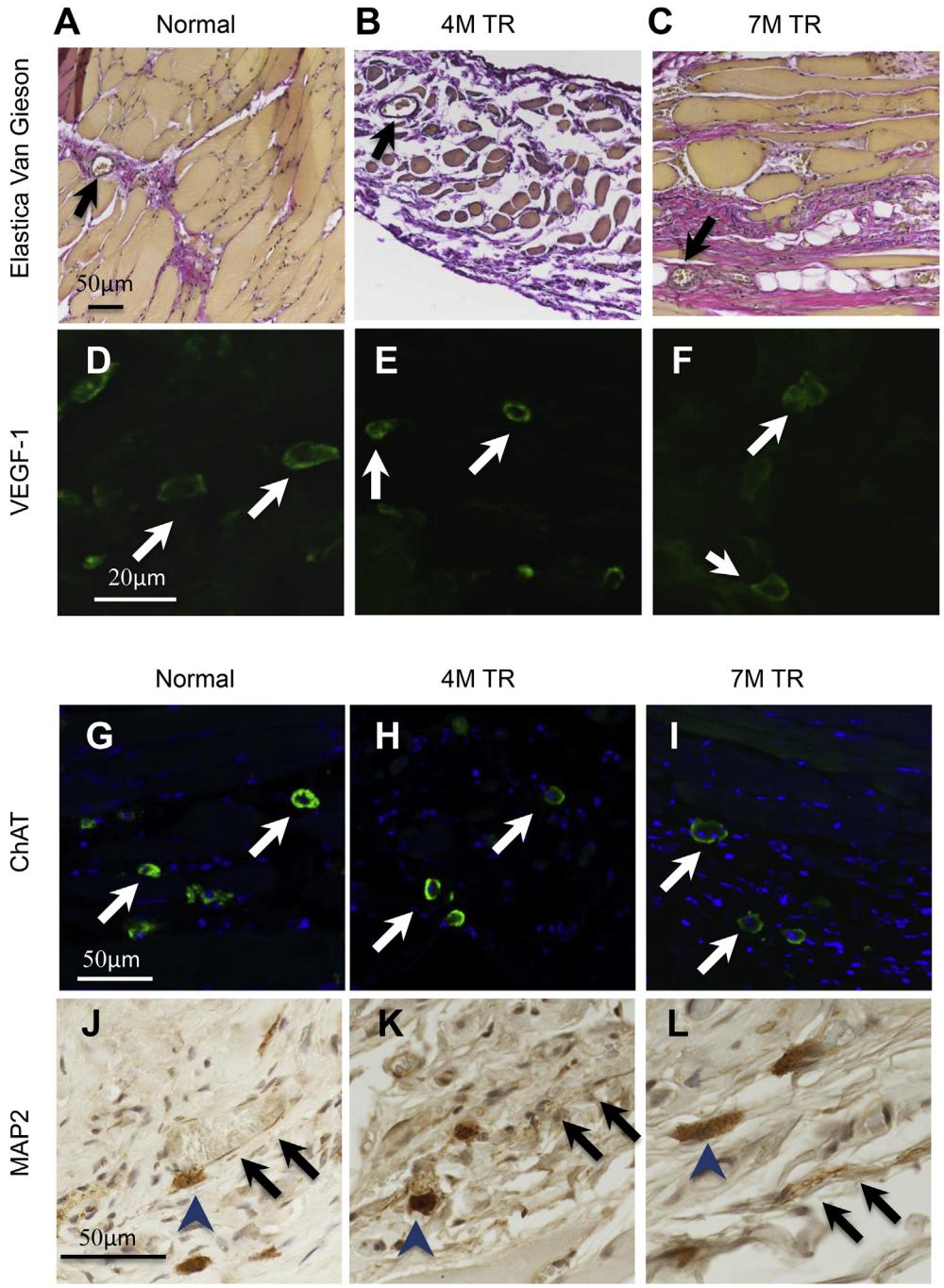

Fig. 6. Presence of vasculature and neurons in reconstructed diaphragm 4 and 7 months after transplantation. (**A**)–(**C**) EVG staining indicates many elastic fibres around muscle in reconstructed diaphragm. Note vessel wall-like structure that contains elastic (arrows). (**D**)–(**F**) Staining for VEGF-1, which is specifically expressed in most vascular endothelial cells. VEGF-1 IR-positive cells (arrows) are observed in reconstructed diaphragm 4 and 7 months after transplantation. (**G**)–(**I**) Staining for ChAT, which is a motor neuron marker. ChAT IR-positive cells are visible (arrows) in reconstructed diaphragm 4 and 7 months after transplantation. (**J**)–(**L**) Staining for MAP2, which is expressed in the cell bodies and axons of neurons. Neuron (arrow head) and axon (arrow) are present in reconstructed diaphragm 4 and 7 months after transplantation.

[25], combining the mesh with seeded bone marrow-derived mesenchymal stem cells. Although no muscular tissue was detected in that study, scattered desmin-positive cells were observed, and autologous fibrous tissue with vascularization was generated at the graft site. Another group used mesh as a scaffold, seeded with autologous amniotic mesenchymal stem cells in a newborn lamb model of CDH [26]. Tensile strength and total collagen levels were significantly higher in the engineered grafts than in acellular bioprosthetic grafts. Decellularized diaphragmatic tissue has also been tested as a scaffold, reseeded with bone marrow mesenchymal stromal cells [27]. However, there have been no reports of grafts that effectively grow with development over the long term in animal models. Considering the potential effects of scaffolds on the tissue microenvironment, development of a scaffold-free technique is highly desirable. In this study, we developed a novel technique using a bio-3D printer-based system to successfully create scaffold-free tissue from MCS, creating large tissue constructs composed only of cells without foreign material.

To create the large tissue constructs with a bio-3D printer-based system, we developed a culture method called Tidal Currents

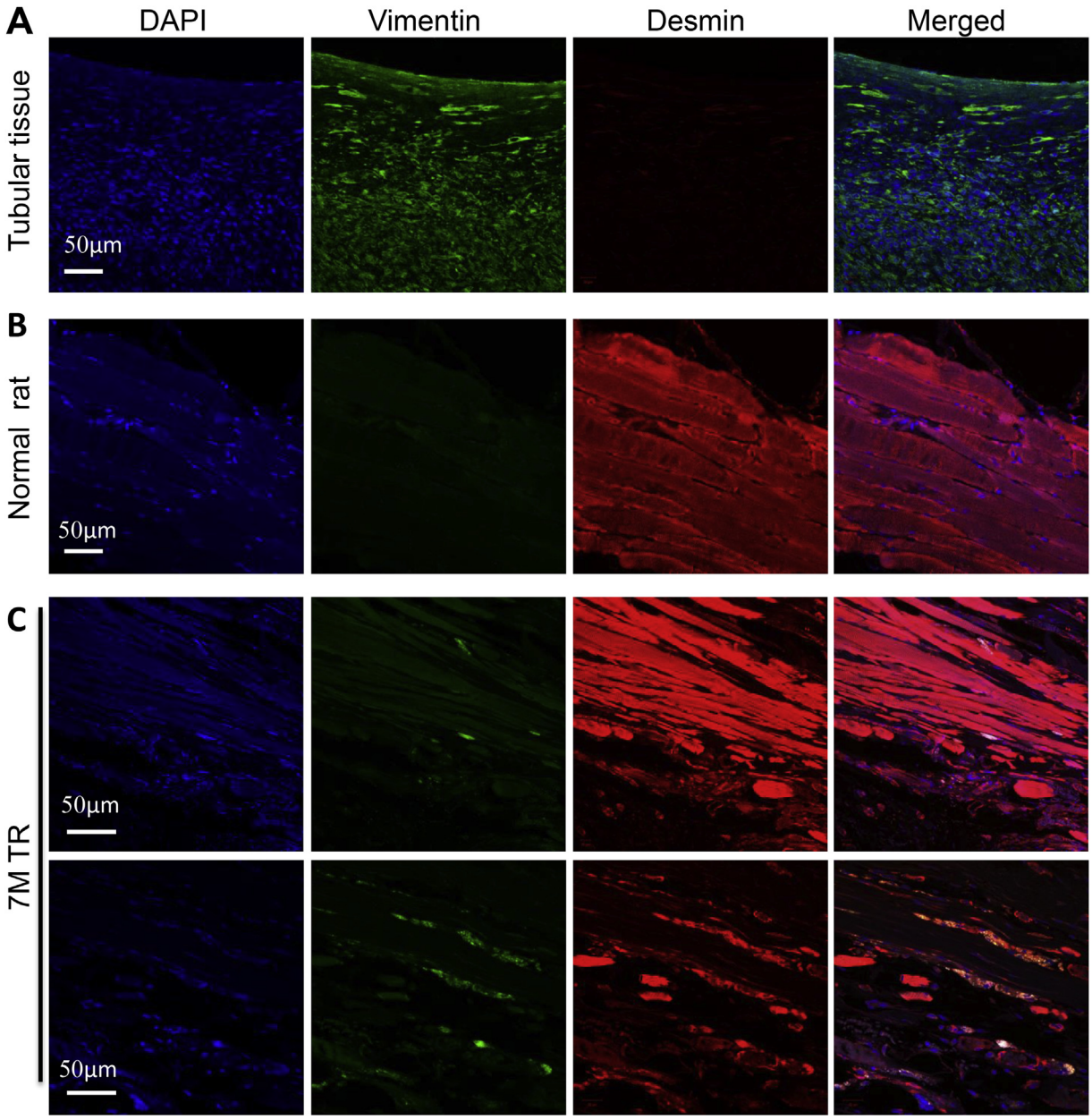

Fig. 7. Immunofluorescence analysis shows presence of vimentin-positive human cells after diaphragm regeneration. (**A**) Staining of tubular tissue composed only of human cells shows vimentin-positive cells. Vimentin recognizes only human cells. Staining for desmin, which only recognizes rat cells, is negative. (**B**) In normal rat diaphragm muscle, desmin-positive rat cells are observed, while vimentin-positive human cells are not present. (**C**) In the reconstructed diaphragm 7 months after transplantation (7 M TR), vimentin-positive human cells are still clearly visible. These cells are localized along the regenerated striated muscle, which stained with desmin (upper panel), and human cells were also localized in the regenerating muscle (lower panel).

Culture, in which we carefully adjusted the flow velocity of the bioreactor. This method allowed adjustment of flow over time to optimize cell culture conditions. Our data show that collagen was released in both the extracellular fluid and the medium in our co-culture of HUVEC and NHDF, and that a complex network formed in the tubular tissue, including microvessels and collagen I (Fig. 3, Supplementary Fig. 3B and C). Our results indicate that microvessels and collagen I are the mechanism by which this co-culture improves cell–cell interactions. Previous studies showed that endothelial cells assure neoangiogenesis and that fibroblasts fill defects and provide extracellular matrix proteins, while myofibroblasts are thought to support the reconstitution of microvessels [28–30]. Collagen fibres and elastic fibres were relatively abundant in the CDH rat model. Regeneration relies on contributions from the microenvironment [31], and we hypothesize that collagen stimulates adhesion between muscle fibres. The extracellular matrix, as an inductive niche [32,33], could promote the recruitment and differentiation of endogenous myogenic progenitor cells [34,35]. Collagen I has the ability to induce cell migration; the process of nerve regeneration requires fibroblasts [36,37]. Thus, in the completely regenerated striated muscle tissue in the rat, the collagen fibres of the cellular patch may have acted as a scaffold, and rat cells activated by growth factors secreted from NHDF and HUVEC (Fig. 7) may have migrated and proliferated there, thereby contributing to muscle, nerve, and blood vessel regeneration of the diaphragm. It is also possible that other factors are associated with diaphragm reconstruction. Understanding the molecular mechanisms of mature muscle reconstruction is an important goal for

future study [38,39]. Elucidation of cell behaviour in recipient animals is another interesting area for future research.

Complete regeneration of nerve and blood vessels required 3–4 months; striated muscle required a longer period of 7 months. Prior to this time, the high elasticity of the cellular patch contributed to its success as a functional diaphragm. For future clinical CDH patients, a key goal is determining how to reduce the culture period to quickly regenerate a complete diaphragm. In a preliminary study, we considered using skeletal stem cells to create tissue for transplantation and attempted to use human skeletal muscle cells and myoblasts (CC-2580, Lonza). However, these cells showed limited differentiation and could not be expanded to large numbers in tissue culture (data not shown). Creation of scaffold-free tissue requires large numbers of cells (total cell count, 9×10^7 cells). In addition, the difficulty of collecting muscle cells from the diaphragm of CDH neonates limits their use, thus, it will be unfeasible for clinical application. In agreement with our data, Kunisaki et al. found that seeded fetal myoblasts quickly lost their myogenic phenotype in vivo [26]. Skeletal muscle regeneration from myogenic cells has been described [34,40]. Thus, we believe that skeletal stem cells remain a potential source for diaphragm regeneration.

A major shortcoming in CDH surgery is the lack of viable replacement materials with the capacity for growth and regeneration. In this experiment, we used human dermal fibroblasts and HUVEC, in consideration of the clinical application. The umbilical cord is a ready-to-use cell source in neonatal CDH patients; a previous study reported that human umbilical cord-derived fibroblasts and endothelial progenitor cells could be used to create living, autologous replacement tissues [41]. Thus, in clinical practice, autologous fibroblasts and endothelial cells can be derived from the umbilical cord and can proliferate relatively quickly; the clinical availability of these cells is an important consideration. In addition, when a diaphragmatic defect is diagnosed prenatally, amniotic fluid stem cells may be obtained via amniocentesis; after birth, stem cells may also be derived from exfoliated deciduous teeth. Muscle connective tissue fibroblasts regulate the development of the diaphragm muscle [42,43]. Thus, to further advance the creation of a physiologically functional diaphragm with novel tissue mesh in newborns and infants, in future studies we should co-culture NHDF and HUVEC, and should add stem cells derived from the amniotic fluid or from human exfoliated deciduous teeth (SHED) [44,45]. Our research group demonstrated the therapeutic potential of stem cells in a rat model of CDH [46].

The main goal of a future study will be to use a medium/large animal, such as a rabbit. We are trying to connect two or three tubular tissues and are using a new Kenzan design to create larger cellular patches (5×6 cm). As described in Supplementary Fig. 2, making MCS required 3 h at room temperature because of the technical limitation of Kenzan needles damaging cells within the spheroids. We are now testing a new Kenzan design that creates larger cellular patches and that does not affect the quality of longer tubular tissue, for use in a future translational study (data not shown). However, a fully cell-based approach will be limited in translational studies because of the massive cell expansion. Muscle tissue engineering can provide support to large congenital skeletal muscle defects using scaffolds that allow cell migration, proliferation, and differentiation; studies have shown that acellular scaffolds may be a suitable option for supporting regeneration and improving the function of diseased muscles [47,48]. In the future, the viability of a cellular patch can be maintained by reinforcing its strength with artificial mesh and reinforcing blood flow by attaching omentum. We are currently considering approaches to address the massive cell expansion problem; solving this problem would allow repair of large diaphragmatic defects and establish the benefits and safety of the technique. Safety observation will be in accordance with the prescribed guideline of the Pharmaceuticals and Medical Devices Agency (PMDA) Medical Device Registration and Approval in Japan, and will include tumourigenicity testing, sterility testing, and mycoplasma detection, thereby contributing to preclinical human studies.

In summary, our results demonstrate that tissue composed only of cells may be created with a bio-3D printer and is a highly safe and effective therapeutic strategy for repairing diaphragmatic defects in a rat model. These findings may pave the road towards clinical trials for a condition that currently has no viable therapeutic options.

5. Conclusion

Synthetic patch repair in neonates with congenital diaphragmatic hernia is associated with a high rate of hernia recurrence and thoracic deformity, because synthetic materials do not grow with the infant. There is a great need in paediatric surgery for large patches that can grow with the individual. Here, we successfully generated large scaffold-free tubular tissue (approximate length, 20 mm; inner diameter, 3 mm; tube wall thickness, 1 mm). We also developed a tidal culture method, creating tubular tissue with high elasticity and tensile strength that could withstand repeated surgical suturing. The tubular tissue was cut to form a cellular patch, which was transplanted into a rat model with a surgically created diaphragmatic defect. After cellular patch transplantation, rats had favourable development with no effects on normal growth. Rats had long-term survival of over 710 days. CT scanning confirmed complete tissue integration of the construct graft during rat growth; hernias did not occur at any time. Histological analysis revealed regeneration of muscle structure, neovascularization, and formation of a neuronal network within the reconstructed diaphragm. The cellular patch technique is not limited to treatment of CDH in the paediatric surgery field; cellular patches could also be used in the treatment of defects in other systems, including congenital structural abnormalities of the small intestine and urinary system. Additional applications are expected.

Contributions

X-Y.Z. Y·Y. T.T. and K. Nakayama designed the study. X-Y.Z. performed and analysed all experiments and helped write the manuscript. Y.Y. and X-Y.Z. performed the surgical procedures, oxygen saturation measurements, and CT data analysis. Z.S. performed histology, immunohistochemistry, fluorescence immunohistochemistry analysis, statistical analysis, and helped write the manuscript. T.T. K. Nakayama, and K. Nagata calibrated the manuscript.

Competing financial interests

K. Nakayama is a co-founder and shareholder of Cyfuse Biomedical KK and an investor/developer designated on the patent for the Bio-3D printer. Patent title: Method for Production of Three Dimensional Structure of Cells; patent number: JP4517125. Patent title: Cell Structure Production Device; patent number: JP5896104.

Acknowledgements

We thank H. Kimura, T. Tamura, K. Urata, and R. Funatsu for their technical assistance. We also thank Rebecca Tollefson, DVM, from Edanz Group (www.edanzediting.com/ac) for editing a draft of this manuscript. This work was supported by grants from JSPS KAKENHI, Japan Grant Number 25253094 to T. Taguchi.

Appendix A. Supplementary data

Supplementary data related to this article can be found at https://doi.org/10.1016/j.biomaterials.2018.03.012.

References

[1] S.M.B.I. Botden, K. Heiwegen, I.A.L.M. van Rooij, H. Scharbatke, P.A. Lally, A. van Heijst, I. de Blaauw, Bilateral congenital diaphragmatic hernia: prognostic evaluation of a large international cohort, J. Pediatr. Surg. 52 (2016) 1475–1479.

[2] R. Teshiba, K. Masumoto, G. Esumi, K. Nagata, Y. Kinoshita, T. Tajiri, T. Taguchi, K. Yamamoto, Identification of TCTE3 as a gene responsible for congenital diaphragmatic hernia using a high-resolution single-nucleotide polymorphism array, Pediatr. Surg. Int. 27 (2011) 193–198.

[3] E.J. Grethel, R.A. Cortes, A.J. Wagner, M.S. Clifton, H. Lee, D.L. Farmer, M.R. Harrison, R.L. Keller, K.K. Nobuhara, Prosthetic patches for congenital diaphragmatic hernia repair: Surgisis vs Gore-Tex, J. Pediatr. Surg. 41 (2006) 29–33.

[4] A. Nasr, M.C. Struijs, S.H. Ein, J.C. Langer, P.P.L. Chiu, Outcomes after muscle flap vs prosthetic patch repair for large congenital diaphragmatic hernias, J. Pediatr. Surg. 45 (2010) 151–154.

[5] J.A. Tovar, Congenital diaphragmatic hernia, Orphanet J. Rare Dis. 7 (2012) 1.

[6] J.C. Lantis, E.K. Gallivan, R. Hekier, R. Connolly, S.D. Schwaitzberg, T. Crombleholme, A comparison of collagen and PTFE patch repair in a rabbit model of congenital diaphragmatic hernia, J. Invest. Surg. 13 (2000) 319–325.

[7] R. Gonzalez, S.J. Hill, S.G. Mattar, E. Lin, B.J. Ramshaw, C.D. Smith, M.L. Wulkan, Absorbable versus nonabsorbable mesh repair of congenital diaphragmatic hernias in a growing animal model, J. Laparoendosc. Adv. Surg. Tech. 21 (2011) 449–454.

[8] K.J. Riehle, D.K. Magnuson, J.H.T. Waldhausen, Low recurrence rate after Gore-Tex/Marlex composite patch repair for posterolateral congenital diaphragmatic hernia, J. Pediatr. Surg. 42 (2007) 1841–1844.

[9] A.C. Gasior, S.D. St Peter, A review of patch options in the repair of congenital diaphragm defects, Pediatr. Surg. Int. 28 (2012) 327–333.

[10] K. Masumoto, K. Nagata, R. Souzaki, T. Uesugi, Y. Takahashi, T. Taguchi, Effectiveness of diaphragmatic repair using an abdominal muscle flap in patients with recurrent congenital diaphragmatic hernia, J. Pediatr. Surg. 42 (2017) 2007–2011.

[11] K. Nagata, N. Usui, K. Terui, H. Takayasu, K. Goishi, M. Hayakawa, Y. Tazuke, A. Yokoi, H. Okuyama, T. Taguchi, Risk factors for the recurrence of the congenital diaphragmatic hernia—report from the long-term follow-up study of Japanese CDH study group, Eur. J. Pediatr. Surg. 25 (2014) 9–14.

[12] N. Tandon, C. Cannizzaro, P.P.-H.G. Chao, R. Maidhof, A. Marsano, H.T.H. Au, M. Radisic, G. Vunjak-Novakovic, Electrical stimulation systems for cardiac tissue engineering, Nat. Protoc. 4 (2009) 155–173.

[13] H.-W. Kang, S.J. Lee, I.K. Ko, C. Kengla, J.J. Yoo, A. Atala, A 3D bioprinting system to produce human-scale tissue constructs with structural integrity, Nat. Biotechnol. 34 (2016) 312–319.

[14] K. Nakayama, In Vitro Biofabrication of Tissues and Organs, Biofabr. William Andrew (2013).

[15] N.I. Moldovan, N. Hibino, K. Nakayama, Principles of the Kenzan method for robotic cell spheroid-based three-dimensional bioprinting, Tissue Eng. B Rev. 23 (2017) 237–244.

[16] M. Itoh, K. Nakayama, R. Noguchi, K. Kamohara, K. Furukawa, Scaffold-free tubular tissues created by a Bio-3D printer undergo remodeling and endothelialization when implanted in rat aortae, PLoS One 10 (2015) 1–15.

[17] Y. Yanagi, K. Nakayama, T. Taguchi, S. Enosawa, T. Tamura, K. Yoshimaru, T. Matsuura, M. Hayashida, K. Kohashi, Y. Oda, T. Yamaza, E. Kobayashi, In vivo and ex vivo methods of growing a liver bud through tissue connection, Sci. Rep. 7 (2017) 14085.

[18] A. Yamashita, M. Morioka, Y. Yahara, M. Okada, T. Kobayashi, S. Kuriyama, S. Matsuda, N. Tsumaki, Generation of scaffoldless hyaline cartilaginous tissue from human iPSCs, Stem Cell Rep. 4 (2015) 404–418.

[19] G.P. Liao, Y. Choi, K. Vojnits, H. Xue, K. Aroom, F. Meng, H.Y. Pan, R.A. Hetz, C.J. Corkins, T.G. Hughes, F. Triolo, A. Johnson, K.J.M. Jr, K.P. Lally, C.S.C. Jr, Y. Li, Tissue engineering to repair diaphragmatic defect in a rat model, Stem Cell. Int. 2017 (2017), 1764523.

[20] Y. Urita, H. Komuro, G. Chen, Evaluation of diaphragmatic hernia repair using PLGA mesh – collagen sponge hybrid scaffold: an experimental study in a rat model, Pediatr. Surg. Int. (2008) 1041–1045.

[21] R.K. Korhonen, S. Saarakkala, Biomechanics and modeling of skeletal soft tissues, Theoretical Biomech. (2011).

[22] G.A. Truskey, Endotheliar cell vascular smooth muscel co-culture assay for high throughput screening assays, Int. J. High Throughput Screen. 2010 (2011) 171–181.

[23] T. Friis, B. Kjaer Sørensen, A.-M. Engel, J. Rygaard, G. Houen, A quantitative ELISA-based co-culture angiogenesis and cell proliferation assay, APMIS 111 (2003) 658–668.

[24] D. Lustrino, W.A. Silveira, F. Wild, Y. Issop, E.O. Connor, D. Cox, M. Reischl, D. Labeit, S. Labeit, E. Benoit, H. Lochmüller, V. Witzemann, I.C. Kettelhut, L.C.C. Navegantes, T. Pozzan, R. Rudolf, M. Majid, D. Lustrino, W.A. Silveira, F. Wild, T. Straka, Y. Issop, Sympathetic innervation controls homeostasis of neuromuscular junctions in health and disease, Proc. Natl. Acad. Sci. 114 (2017). E5277–E5277.

[25] C.G. Turner, J.D. Klein, S.A. Steigman, M. Armant, G.A. Nicksa, D. Zurakowski, J. Ritz, D.O. Fauza, Preclinical regulatory validation of an engineered diaphragmatic tendon made with amniotic mesenchymal stem cells, J. Pediatr. Surg. 46 (2011) 57–61.

[26] S.M. Kunisaki, J.R. Fuchs, A. Kaviani, J.T. Oh, D.A. LaVan, J.P. Vacanti, J.M. Wilson, D.O. Fauza, Diaphragmatic repair through fetal tissue engineering: a comparison between mesenchymal amniocyte- and myoblast-based constructs, J. Pediatr. Surg. 41 (2006) 34–39.

[27] E.A. Gubareva, S. Sjöqvist, I.V. Gilevich, A.S. Sotnichenko, E.V. Kuevda, M.L. Lim, N. Feliu, G. Lemon, K.A. Danilenko, R.Z. Nakokhov, I.S. Gumenyuk, T.E. Grigoriev, S.V. Krasheninnikov, A.G. Pokhotko, A.A. Basov, S.S. Dzhimak, Y. Gustafsson, G. Bautista, A. Beltrán Rodríguez, V.M. Pokrovsky, P. Jungebluth, S.N. Chvalun, M.J. Holterman, D.A. Taylor, P. Macchiarini, Orthotopic transplantation of a tissue engineered diaphragm in rats, Biomaterials 77 (2016) 320–335.

[28] R. Walser, W. Metzger, A. Görg, T. Pohlemann, M.D. Menger, M.W. Laschke, Generation of co-culture spheroids as vascularisation units for bone tissue engineering, Europ. Eells Mater. 26 (2013) 222–233.

[29] M. Oberringer, C. Meins, M. Bubel, T. Pohlemann, A new in vitro wound model based on the co-culture of human dermal microvascular endothelial cells and human dermal fibroblasts, J Mol Hist 99 (2007) 197–207.

[30] M. Oberringer, C. Meins, M. Bubel, T. Pohlemann, In vitro wounding: effects of hypoxia and transforming growth factor b 1 on proliferation, migration and myofibroblastic differentiation in an endothelial cell-fibroblast co-culture model, Biol. Cell (2008) 37–47.

[31] C. Lepper, S. Low, T.A. Partridge, The satellite cell builds its nest under notch's guidance, Cell Stem Cell. 11 (2012) 443–444.

[32] S.A. Steigman, J. Oh, N. Almendinger, P. Javid, D. Lavan, D. Fauza, Structural and biomechanical characteristics of the diaphragmatic tendon in infancy and childhood: an initial analysis, J. Pediatr. Surg. 45 (2010) 1455–1458.

[33] S. Kuang, M.A. Gillespie, M.A. Rudnicki, Niche regulation of muscle satellite cell self-renewal and differentiation, Cell Stem Cell. 2 (2008) 22–31.

[34] B.M. Sicari, C.L. Dearth, S.F. Badylak, Tissue engineering and regenerative medicine approaches to enhance the functional response to skeletal muscle injury, Anat. Rec. 297 (2014) 51–64.

[35] K.H. Vining, D.J. Mooney, Mechanical forces direct stem cell behaviour in development and regeneration, Nat. Rev. Mol. Cell Biol. (2017).

[36] S. Parrinello, I. Napoli, S. Ribeiro, P.W. Digby, M. Fedorova, D.B. Parkinson, R.D.S. Doddrell, M. Nakayama, R.H. Adams, A.C. Lloyd, EphB signaling directs peripheral nerve regeneration through Sox2-dependent Schwann cell Sorting, Cell 143 (2010) 145–155.

[37] L. Crigler, R.C. Robey, A. Asawachaicharn, D. Gaupp, D.G. Phinney, Human mesenchymal stem cell subpopulations express a variety of neuro-regulatory molecules and promote neuronal cell survival and neuritogenesis, Exp. Neurol. 198 (2006) 54–64.

[38] H. Yin, F. Price, M.A. Rudnicki, Satellite cells and the muscle stem cell niche, Physiol. Rev. (2013) 23–67.

[39] C.F. Bentzinger, Y.X. Wang, N.A. Dumont, M.A. Rudnicki, Cellular dynamics in the muscle satellite cell niche, Nat. Publ. Gr 14 (2013) 1062–1072.

[40] C.A. Rossi, M. Pozzobon, P. De Coppi, Advances in musculoskeletal tissue engineering, Organogenesis 6 (2010) 167–172.

[41] A. Mol, S. Neuenschwander, C. Breymann, M. Go, G. Zund, M. Turina, S.P. Hoerstrup, Living patches engineered from human umbilical cord derived fibroblasts and endothelial progenitor cells, Eur. J. Cardio. Thorac. Surg. 27 (2018) 795–800.

[42] G. K, A.J. Merrell, B.J. Ellis, Z.D. Fox, J.A. Lawson, J.A. Weiss, Muscle connective tissue controls development of the diaphragm and is a source of congenital diaphragmatic hernias, Nat. Genet. 47 (2015) 496–504.

[43] M.M. Murphy, J.A. Lawson, S.J. Mathew, D.A. Hutcheson, G. Kardon, Satellite cells, connective tissue fibroblasts and their interactions are crucial for muscle regeneration, Development 3637 (2011) 3625–3637.

[44] P. Bossolasco, T. Montemurro, L. Cova, S. Zangrossi, C. Calzarossa, S. Buiatiotis, D. Soligo, S. Bosari, V. Silani, G.L. Deliliers, P. Rebulla, L. Lazzari, Molecular and phenotypic characterization of human amniotic fluid cells and their differentiation potential, Cell Res. 16 (2006) 329–336.

[45] H. Kato, T.T.M. Pham, H. Yamaza, K. Masuda, Y. Hirofuji, X. Han, H. Sato, T. Taguchi, K. Nonaka, Mitochondria regulate the differentiation of stem cells from human exfoliated deciduous teeth, Cell Struct. Funct. (2017).

[46] R. Yuniartha, F.S. Alatas, K. Nagata, M. Kuda, Y. Yanagi, G. Esumi, T. Yamaza, Y. Kinoshita, T. Taguchi, Therapeutic potential of mesenchymal stem cell transplantation in a nitrofen-induced congenital diaphragmatic hernia rat model, Pediatr. Surg. Int. 30 (2014) 907–914.

[47] M. Piccoli, L. Urbani, M.E. Alvarez-fallas, C. Franzin, A. Dedja, E. Bertin, G. Zuccolotto, A. Rosato, P. Pavan, N. Elvassore, P. De Coppi, M. Pozzobon, Biomaterials Improvement of diaphragmatic performance through orthotopic application of decellularized extracellular matrix patch, Biomaterials 74 (2016) 245–255.

[48] E.F. Maughan, R.E. Hynds, T.J. Proctor, S.M. Janes, M. Elliott, M.A. Birchall, M.W. Lowdell, P. De Coppi, Autologous cell seeding in tracheal tissue engineering, Curr Stem Cell Rep (2017) 279–289.